Letter

Quasicrystalline Weyl points and dense Fermi-Bragg arcs

André Grossi e Fonseca [1,*] Thomas Christensen [1,2,†] John D. Joannopoulos,[1] and Marin Soljačić [1]

[1]*Department of Physics, Massachusetts Institute of Technology, Cambridge, Massachusetts 02139, USA*
[2]*Department of Photonics and Electrical Engineering, Technical University of Denmark, Lyngby 2800, Denmark*

We introduce a general mechanism for obtaining Weyl points in a stack of two-dimensional (2D) quasicrystals, which can be extended to any stack of aperiodic layers. We do so by driving a topological phase transition with the vertical crystal momentum as the tuning parameter, which leads to gap closures at the critical points sourcing Berry curvature. To illustrate, we use a simple 3D generalization of the Qi-Wu-Zhang model defined on a Penrose quasicrystal. The presence of Weyl points is established via the local Chern marker, projected band structure, and density of states. Interestingly, we uncover an analog of Fermi arcs in the quasicrystalline setting, which we deem Fermi-Bragg arcs, densely distributed lines connecting the band degeneracies and indexed by the Bragg peaks. Signatures of such surface states in quantum oscillations and the prospect of a fully quasicrystalline Weyl system are also discussed. The flexibility of our proposal brings opportunities for realizing other gapless topological phases in aperiodic systems, paving the way for a significantly expanded role for topological band theory.

The past decades have seen the development of a broad understanding of band theory from topological perspectives in both quantum [1,2] and classical [3–5] crystalline systems. This understanding includes both gapped phases such as Chern insulators [6], topological insulators [7,8], and topological crystalline insulators [9], and gapless phases including Dirac [10] and Weyl [11] points and nodal lines [12]. With the recent introduction of several real-space formulations of topological invariants [13–16], the assumption of lattice periodicity has been relaxed for several classes of gapped [17–19] and metallic [20] topological phases. In this Research Letter, we show that gapless topological phases also do not fundamentally rely on crystallinity by direct construction of a model with spin-1/2 Weyl points in a stack of quasicrystals.

Weyl points represent perhaps the simplest three-dimensional (3D) gapless topological phase. Introduced by Weyl in 1929 [21] as the massless solutions of the Dirac equation, they were experimentally realized nearly 80 years later in TaAs [22,23] and double gyroid photonic crystals [24]. In crystalline settings, they correspond to solutions of the Weyl Hamiltonian $H(\mathbf{k}) = v_x k_x \sigma_x + v_y k_y \sigma_y + v_z k_z \sigma_z$, with k_i, v_i, and σ_i denoting the components of the crystal momentum, group velocity, and Pauli matrix vector, respectively, and exhibit a gapless linear dispersion. Their associated Fermi-arc surface states [25], connection to high-energy physics [26], and unique optical properties [27,28] have fueled intense interest. More fundamentally, Weyl points are key conceptual building blocks of many topological phenomena, since they act as monopole sources and sinks of Berry curvature [11,29]; we take this to be their defining attribute throughout this Research Letter.

Nonetheless, the understanding and realization of Weyl points remain firmly rooted in **k**-space centered perspectives. Aperiodic generalizations of Weyl physics have recently been discussed but are restricted to weak quasiperiodic perturbations of a crystalline starting point [30–32]. Here, we move beyond this perturbative paradigm by introducing a general mechanism for realizing Weyl points in a stack of inherently quasicrystalline Hamiltonians, and discuss their associated bulk and boundary signatures. Our approach, generalizable to any family of aperiodic Hamiltonians, relies on a simple idea, borrowed from the crystalline setting: Any two distinct two-dimensional (2D) manifolds separated by a single Weyl point must be characterized by Chern numbers differing by the enclosed Weyl point chirality [29]. We exploit this fact by driving a band inversion which changes the Chern number of a quasicrystalline bulk 2D Hamiltonian. We take the parameter controlling the topological transition to be crystal momentum k_z associated with stacking in the z direction, which leads to the emergence of Weyl points at the inversion points (Fig. 1). We illustrate our idea in a simple tight-binding Hamiltonian defined on vertices of a Penrose tiling [33] with a k_z-varying mass term, which captures the essential features of our proposal. The bulk signatures of the associated Weyl points are consistent with those of the crystalline setting, as we establish explicitly via the local Chern marker [13], bulk energy dispersion, and density of states. Interestingly, we uncover a quasicrystalline version of Fermi arcs which we call Fermi-Bragg arcs, whose characteristics sharply distinguish them from their crystalline counterparts: They are densely distributed [34] in Fourier space and terminate at vertical lines through the Bragg peaks of the diffraction spectrum.

a. Model and topology. Our construction begins with a 2D quasicrystal. Concretely, we consider a tight-binding model defined on the vertices of a Penrose tiling [33], a small section of which is shown in Fig. 1(a). Because we will
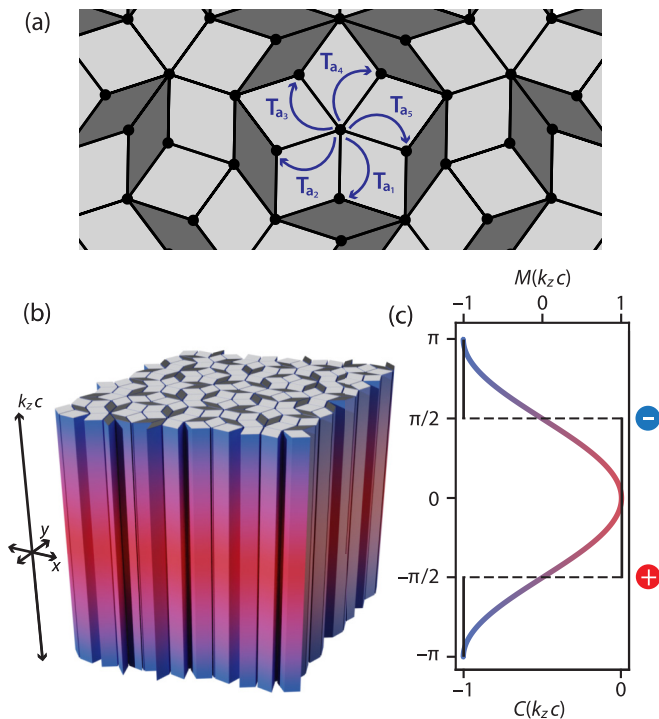
*agfons@mit.edu
†thomas@dtu.dk

FIG. 1. Mechanism for Weyl points in a quasicrystal stack. (a) Top view of a small section of a Penrose quasicrystal, with fat and skinny rhombi in light and dark gray, respectively. Excitations hop between vertices along the edges of adjacent rhombi with amplitudes $\mathbf{T_a}$ given by Eq. (1). The possible hopping vectors are $\mathbf{a}_j = (\sin 2\pi j/5, \cos 2\pi j/5)a$, $j = 1, \ldots, 5$ with bond length a. (b) 3D generalization of (a), obtained by sinusoidally varying the mass term M of Eq. (1) over the out-of-plane crystal momentum k_z with real-space period c, as indicated by the color gradient. (c) Mass parameter M (with $M_0 = 1$) and expected Chern number C as a function of k_z. C changes by ± 1 when M changes sign, indicating the presence of a Weyl point with chirality ± 1 (circles).

consider both open and periodic boundary conditions (OBCs and PBCs), we construct the quasicrystal through Penrose tiling approximants [35], finite supercells of increasing order n that systematically approximate the Penrose quasicrystal as $n \rightarrow \infty$ while restricting the number of defects to two per unit cell (corresponding to edges along which the matching rules are violated) [36]. The number of vertices at order n is $F_{2n+3} + F_{2n+5}$, where F_n is the nth Fibonacci number [37] (Supplemental Material, Sec. S1 [38]; see also Refs. [39–44] therein).

We couple the vertices of this lattice via a generalized Qi-Wu-Zhang (QWZ) model [45] [Fig. 1(a)], whose two-band phase diagram exhibits Chern phases. The real-space tight-binding Hamiltonian takes the form [46]

$$H_{\text{QWZ}}(M) = t \sum_{\mathbf{R}} \left[c_{\mathbf{R}}^\dagger \boldsymbol{\epsilon}(M) c_{\mathbf{R}} + \sum_{\mathbf{a}} c_{\mathbf{R}}^\dagger \mathbf{T_a} c_{\mathbf{R}+\mathbf{a}} \right], \quad (1a)$$

$$\boldsymbol{\epsilon}(M) = (2 + M)\sigma_z, \quad \mathbf{T_a} = \frac{1}{2} \begin{pmatrix} 1 & ie^{-i\theta_\mathbf{a}} \\ ie^{i\theta_\mathbf{a}} & -1 \end{pmatrix}, \quad (1b)$$

where $c_{\mathbf{R}}^\dagger = (c_{\mathbf{R},1}^\dagger, c_{\mathbf{R},2}^\dagger)$, with $c_{\mathbf{R},\alpha}^\dagger$ creating an excitation at site $\mathbf{R}$ and site degree of freedom α, t is the overall hopping

amplitude, and the sum runs over all vertex positions $\mathbf{R}$ of the quasicrystal and neighbors connected to $\mathbf{R}$ by a rhombus edge with vector $\mathbf{a}$. Finally, $\theta_\mathbf{a}$ is the angle of the edge $\mathbf{a}$ with the x axis, and M is a mass parameter controlling the topological phase, corresponding physically to an on-site potential staggering. Note that the Hamiltonian is Hermitian, although the hopping matrices $\mathbf{T_a}$ are not. Concretely, the QWZ model can be realized, e.g., with spin-orbit coupled s orbitals and ferromagnetic moments as the site degrees of freedom [47]. On a square lattice, it undergoes topological phase transitions at $M = -4$, -2, and 0 (Supplemental Material, Sec. S4 A [38]). In particular, the Chern number C of the valence band changes from -1 to 0 when M changes sign from negative to positive. The choice of the QWZ model is chiefly motivated by simplicity: Our main qualitative conclusions only require certain topological phase transitions.

To compute the topological phase diagram in our quasicrystalline setting, we require a notion of Chern numbers that does not rely on crystal momentum. We adopt the formalism of the local Chern marker [13], which defines a Chern amplitude $\mathcal{C}_i$ at each lattice site i with coordinates (x_i, y_i) as [48]

$$\mathcal{C}_i = -\frac{4\pi}{\Omega} \text{Im} \left[\sum_j \langle i | x_\mathcal{Q} | j \rangle \langle j | y_\mathcal{P} | i \rangle \right], \quad (2a)$$

where

$$\langle i | x_\mathcal{Q} | j \rangle = \sum_k \mathcal{Q}_{ik} x_k \mathcal{P}_{kj}, \quad \langle j | y_\mathcal{P} | i \rangle = \sum_k \mathcal{P}_{jk} y_k \mathcal{Q}_{ki}, \quad (2b)$$

$$\mathcal{P} = \sum_{\varepsilon_n < \varepsilon_\text{F}} |\psi_n\rangle\langle\psi_n|, \quad \mathcal{Q} = \mathbf{1} - \mathcal{P}, \quad (2c)$$

with Ω denoting the unit cell area, which for the Penrose quasicrystal we take to be the weighted average of the fat and skinny rhombus areas (Supplemental Material, Sec. S2 [38]), and $|\psi_n\rangle$ being an eigenstate of index n and energy ε_n.

For a finite system, the local Chern marker averaged over all lattice sites vanishes [13]. The average over a finite bulk region, however, is well quantized and converges to the conventional Chern number in the thermodynamic limit [48]. For concreteness, we define this average over a disk D of radius R containing N sites:

$$\mathcal{C}_D = \frac{1}{N} \sum_{i \in D} \mathcal{C}_i. \quad (3)$$

In practice, we choose R large enough to avoid microscopic fluctuations but small enough to be restricted to the bulk (Supplemental Material, Sec. S2 [38]). Similarly to the square-lattice setting, we observe that the averaged Chern marker of the valence band in the quasicrystalline QWZ model, within small fluctuations, is quantized to -1 for $M < 0$ and to 0 for $M > 0$, changing value near $M = 0$.

Given these observations, we extend the 2D quasicrystalline QWZ model in a third, periodic dimension (z) of period c. Specifically, we imagine stacking 2D quasicrystal layers along z in such a manner that the mass varies sinusoidally in the crystal momentum k_z, as illustrated in Figs. 1(c) and 1(d). This leads to a simple 3D extension of the QWZ Hamiltonian:

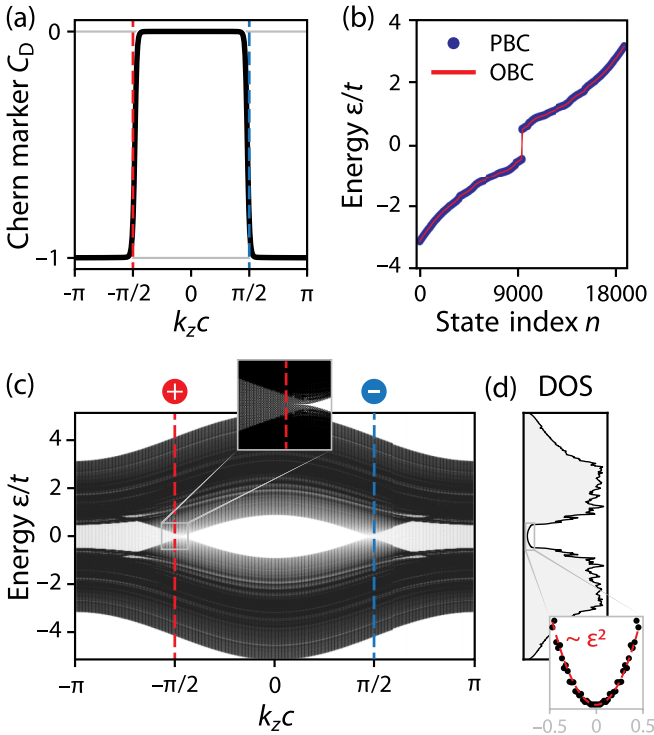$$H(k_z) = H_{\text{QWZ}}(M_0 \cos k_z c). \quad (4)$$

FIG. 2. Bulk signatures of quasicrystalline Weyl points. (a) Disk-averaged Chern marker $\mathcal{C}_D$ for the valence band of k_z slices of $H(k_z)$ (disk radius $R = 12a$). Topological phase transitions occur at $k_z c \approx \pm \pi/2$. (b) The energy spectrum $\varepsilon_n(k_z)$ of $H(k_z)$ at $k_z c = \pi$, as a function of state index n. While the spectrum is gapped under PBCs, a band of in-gap chiral edge states appears under OBCs, implying a nontrivial Chern number. (c) Projected band structure under OBCs as a function of k_z. For $|k_z c| \lesssim \pi/2$, the system is gapped, whereas for $|k_z c| \gtrsim \pi/2$ edge states populate the bulk gap, as shown in the inset. Red dashed lines indicate the gap-closing points for a square lattice. (d) DOS under PBCs, displaying a quadratic energy dependence near zero energy (inset: quadratic fit shown as a red dashed line). (a) and (b)–(d) were computed from Penrose tiling approximants of order $n = 6$ (3571 sites) and $n = 7$ (9349 sites), respectively.

The mass amplitude M_0 controls the number of phase transitions in k_z (Supplemental Material, Sec. S4 [38]): For simplicity, we take $M_0 = 1$ going forward. The model has neither inversion nor time-reversal symmetry—the latter is broken by the off-diagonal elements of $\mathbf{T_a}$—but the out-of-plane mirror symmetry leads to Weyl point pairs at $\pm k_z$. In addition, sublattice symmetry and the two-band nature of the model pin all Weyl points to zero energy. The expected phase diagram—the evolution of the Chern number $C(k_z)$ with k_z—is shown schematically in Fig. 1(c). As we will show, the associated phase transition points $k_z^\pm \approx \pm \pi/2c$ are accompanied by band closings, each corresponding to a Weyl point of chirality $\chi^\pm = \lim_{\delta \to 0^+} C(k_z^\pm + \delta) - C(k_z^\pm - \delta) = \mp 1$.

b. Bulk signatures. We now consider the bulk features of our 3D model in detail by numerically solving Eq. (4) for large Penrose quasicrystal tilings (Fig. 2), identifying two well-known bulk signatures of Weyl points. First, the disk-averaged local Chern marker $\mathcal{C}_D(k_z)$ [Fig. 2(a)] exhibits sharp topological phase transitions at $k_z c \approx \pi/2$ where the mass parameter $M(k_z)$ changes sign, in excellent agreement with

our qualitative expectations. Interestingly, the phase transition point at $M \approx 0$ agrees with that of the square lattice, suggesting that this aspect is largely independent of lattice details. The valence band of $H(k_z)$ has $\mathcal{C}_D = -1$ for $|k_z c| \gtrsim \pi/2$, and is otherwise trivial. Figure 2(b) shows the spectrum of $H(k_z)$ at $k_z c = \pi$. Under PBCs, the spectrum shows a clear bulk gap; under OBCs, this gap is bridged by chiral edge modes, consistent with a Chern phase.

We also computed the full spectrum of $H(k_z)$ as a function of k_z under OBCs, shown in Fig. 2(c). The existence of a small but finite gap is due to finite-size effects, vanishing in the limit of increasing quasicrystal tiling order $n \to \infty$ (Supplemental Material, Sec. S3 [38]). In this limit, the spectrum therefore hosts a linear gapless dispersion near the degeneracy points, which constitutes the second bulk signature. Finally, since both trivial and nontrivial k_z slices of the spectrum share an overlapping gap, the band crossings are well isolated from other bulk states and their density of states (DOS) can consequently be probed in isolation. This allows for the identification of a third bulk signature of Weyl points: their well-known form $\text{DOS}(\varepsilon) \propto \varepsilon^2$ under PBCs [Fig. 2(d)].

c. Surface signatures and Fermi-Bragg arcs. A hallmark of Weyl points in crystals is the presence of anomalous surface states deemed Fermi arcs. A consequence of the bulk-boundary correspondence, they are arclike Fermi surfaces that connect the projections of Weyl points on the surface Brillouin zone (BZ) [25].

In our quasicrystalline setting, with only periodicity in z, we lack a simple surface BZ equivalent. Instead, we imagine an angle-resolved diffraction measurement on an exposed surface of our quasicrystal stack, say, a (100) termination spanning the (y, z) plane, resolved in crystal momentum k_z along z and in Fourier momentum q_y along y [Fig. 3(a)]. Lacking periodicity in y, q_y is unambiguously defined in the infinite domain $(-\infty, \infty)$, rather than the finite domain $[0, 2\pi/c)$ of k_z. For a y-periodic system, q_y simply maps to infinite adjacent copies of the BZ along y in an extended zone scheme (Supplemental Material, Sec. S7 A [38]). We may then evaluate the spectral density of states $\text{SDOS}(x, q_y, k_z; \varepsilon)$—i.e., the x-position-, q_y-Fourier-component-, and k_z-crystal-momentum-resolved DOS. Physically, $\text{SDOS}(x, q_y, k_z; \varepsilon)$ dictates the DOS to which an incident plane wave $\sim e^{ik_z z} e^{iq_y y}$ of energy ε can couple at position at x. Figure 3(b) shows the spectral DOS for our quasicrystal stack, evaluated at the x boundary of a (100) surface termination and at $\varepsilon = 0$ (where bulk contributions vanish). A rich structure of vertical arcs of varying intensities appears in q_y, all connecting the projections of Weyl points at approximately $\pm \pi/2c$ across k_z.

To interpret the appearance of such arcs, we first draw an analogy with the crystalline square-lattice case. When considered in an extended zone scheme, a conventional crystal with Weyl points also exhibits multiple Fermi arcs, with each arc associated with a copy of the first BZ, generated by a shift by a reciprocal lattice vector (Supplemental Material, Sec. S7 A [38]). Each such Fermi-arc copy can consequently be labeled by a two-dimensional integer vector, i.e., the Miller indices. Equivalently, each BZ and arc copy is associated with a specific Bragg peak of the structure factor $S(\mathbf{q}) \propto |\sum_{\mathbf{R}} e^{i\mathbf{q} \cdot \mathbf{R}}|^2$ (lattice sites $\mathbf{R}$). Motivated by this, we plot $S(\mathbf{q})$ for the
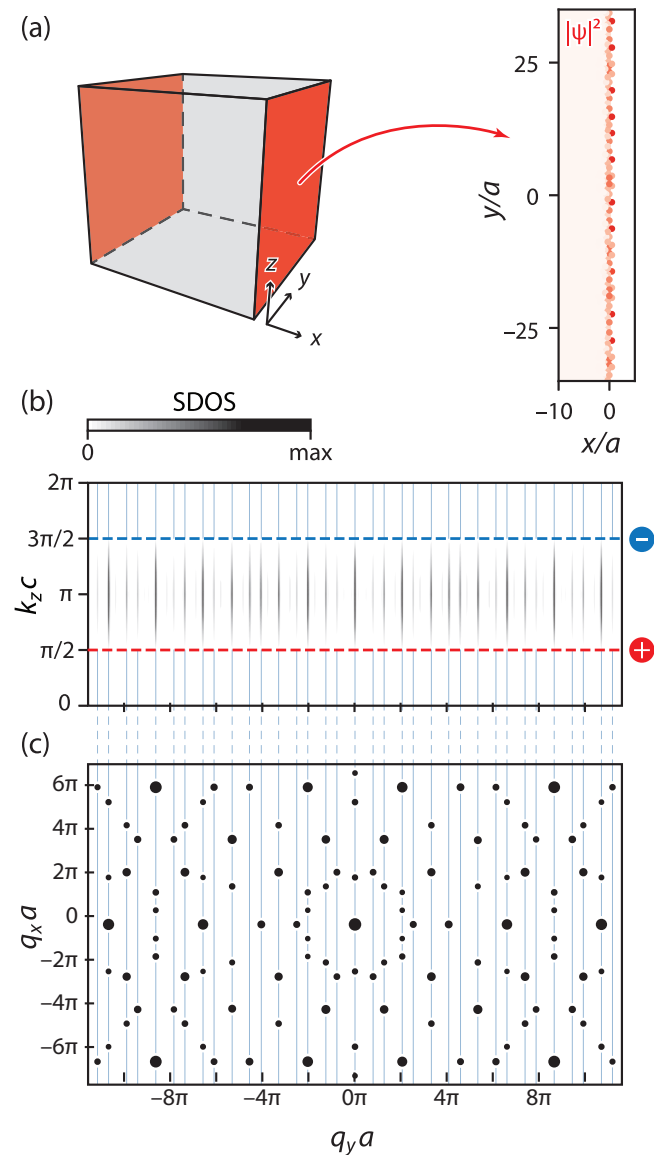
FIG. 3. Surface signatures of Weyl points in real and momentum space. (a) Upon imposing OBCs in both x and y and zooming into the x boundary, we observe localized edge modes for values of k_z in the topological regime (edge state shown for $k_z c = \pi$ on a linear color scale). (b) Spectral DOS at the x boundaries. Horizontal red and blue dashed lines bound the topological region $\pi/2 < k_z c < 3\pi/2$, showing that arcs connect Weyl points of opposite chirality. (c) Structure factor in Fourier space (only the brightest spots are shown, and spot size is proportional to intensity). Vertical blue lines show that q_y projections of Bragg peaks precisely line up with Fermi arcs. (a)–(c) were computed from Penrose tiling approximants of order $n = 6$ (3571 sites).

Penrose tiling in Fig. 3(c). We see perfect alignment of the spectral arcs with the Bragg peaks' q_y positions—as well as some correlation of spectral DOS and structure factor intensities. Due to this correspondence, we call the associated surface states Fermi-Bragg arcs. We note that the arcs' verticality in k_z is due to the simplicity of our tight-binding model; for more general hoppings, the arcs curve—but their terminations remain pinned to the Bragg peaks (Supplemental Material, Sec. S7 A [38]). Each of these arcs can be labeled by a family

of generalized Miller indices, each a five-dimensional integer vector stemming from the 5D hypercube from which the Penrose quasicrystal is generated (Supplemental Material, Sec. S6 [38]). In this perspective, the Fermi-Bragg arcs are analogous to conventional Fermi arcs, but now densely distributed rather than periodically, a feature inherited from the dense structure factor of quasicrystals [49]. Furthermore, the absence of translational symmetry implies that arcs will generically have different lengths in momentum space, leading to a series of incommensurate peaks in the Fourier transform of a Shubnikov–de Haas measurement (Supplemental Material, Sec. S7 B [38]).

d. Real-space model. The Hamiltonian of our quasicrystal stack in Eq. (4) is in a mixed-coordinate form, with in-plane (quasicrystalline) coupling defined in (x, y) space and out-of-plane (periodic) coupling defined in k_z space. To understand how the model can be realized in practice, we transform the k_z dependence to a z dependence by an inverse Fourier transform (Supplemental Material, Sec. S5 [38]) and find that it is equivalent to a stack of quasicrystal layers tuned to the critical $M = 0$ point with diagonal interlayer hopping (i.e., between identical layer degrees of freedom). However, neither fine-tuning of M nor the restriction to diagonal hopping is strictly necessary (Supplemental Material, Sec. S5 B [38]): Off-diagonal mixing and small detunings away from $M = 0$ simply shift the Weyl points in k_z. The simplicity of our proposal—i.e., stacking of layers near a Dirac point phase transition in addition to time-reversal breaking—indicates that the specific details of the QWZ couplings and Penrose tiling may be inessential to the relevant physics, and suggests significant leeway in experimental implementations. Opportunities in an electronic setting include magnetic decagonal quasicrystals [50], stacks of magnetic thin films [51], or magnetically doped layers [52]. We also highlight classical implementations in photonic platforms, exploiting gyromagnetic [53,54] or gyroelectric [55] responses, but also more broadly, e.g., in mechanics [56] or acoustics [57]. This simplicity may also guide the way to time-reversal-invariant realizations of quasicrystalline Weyl points [58–60].

e. Discussion and outlook. In this Research Letter, we have proposed a general mechanism for obtaining a gapless topological phase—Weyl points specifically—in a noncrystalline setting by driving a 2D quasicrystalline Hamiltonian through a topological phase transition. To illustrate the mechanism, we introduced a simple 3D generalization of the QWZ model on a Penrose quasicrystal stack. The model hosts pairs of Weyl points, as we verify by identifying several distinct signatures. From the bulk perspective, we evaluate the phase diagram of the local Chern marker and find topological phase transitions with associated linear energy dispersion and quadratic DOS dependence, all consistent with the existence of bulk Weyl points. From the surface perspective, we find an analog of Fermi arcs, which we call Fermi-Bragg arcs, characterized by densely distributed arclike structures terminating at the Bragg peaks of the diffraction spectrum. These characteristics are expected to be universal for Weyl points in quasicrystals and pose an exciting opportunity for experimental observation. Furthermore, the simplicity of our model in real space suggests that quasicrystalline Weyl points could exist in much more general settings; the recent observations of 3D band

crossings in a stack of $Ta_{1.6}Te$ quasicrystal layers [58] and the proposed explanation of optical conductivity features in 3D quasicrystals in terms of a Weyl phase [59] are interesting outlooks to this.

An important remaining question is whether a *fully* quasicrystalline system can host Weyl points, i.e., whether the out-of-plane periodicity can be replaced by a quasicrystalline dimension as well. We argue that it can and is possible to realize with outset in our model: For example, we may imagine adiabatically breaking periodicity along z by introducing a quasicrystalline modulation, e.g., an Aubry-André potential [61]. Even though a generic aperiodic weak perturbation leads to a finite, albeit exponentially small, density of states at crystalline Weyl points [62,63], it has been shown both numerically [30] and analytically [31] that the semimetallic phase is robust to modest quasiperiodic perturbations. Meanwhile, certain bulk signatures, e.g., the DOS, should remain unaffected, since there are no bulk bands that can obscure the Weyl points, assuming sufficiently weak potentials. In this scenario, we expect the Fermi-Bragg arcs to be even richer and densely distributed across all surface diffraction planes. Although k_z is no longer well defined in a fully aperiodic setting, real-space methods such as the spectral localizer [64,65] would remain suitable to track the number of Berry monopoles.

An exciting outlook is to use a nonperiodic mass term, realized, e.g., through a synthetic dimension, which would allow simultaneously breaking z periodicity and potential violations of the Nielsen-Ninomiya theorem [66,67]. More broadly, our recipe for realizing gapless topology in a quasicrystalline setting may serve as a starting point for more exotic topological phases, such as those protected by noncrystallographic point group symmetries or endowed with higher topological charges or degeneracies, thereby complementing the zoo of crystalline topological quasiparticles [68–70].

[1] M. Z. Hasan and C. L. Kane, Colloquium: Topological insulators, Rev. Mod. Phys. **82**, 3045 (2010).

[2] N. R. Cooper, J. Dalibard, and I. B. Spielman, Topological bands for ultracold atoms, Rev. Mod. Phys. **91**, 015005 (2019).

[3] L. Lu, J. D. Joannopoulos, and M. Soljačić, Topological photonics, Nat. Photon. **8**, 821 (2014).

[4] T. Ozawa, H. M. Price, A. Amo, N. Goldman, M. Hafezi, L. Lu, M. C. Rechtsman, D. Schuster, J. Simon, O. Zilberberg, and I. Carusotto, Topological photonics, Rev. Mod. Phys. **91**, 015006 (2019).

[5] G. Ma, M. Xiao, and C. T. Chan, Topological phases in acoustic and mechanical systems, Nat. Rev. Phys. **1**, 281 (2019).

[6] F. D. M. Haldane, Model for a Quantum Hall Effect without Landau Levels: Condensed-Matter Realization of the "Parity Anomaly", Phys. Rev. Lett. **61**, 2015 (1988).

[7] L. Fu, C. L. Kane, and E. J. Mele, Topological Insulators in Three Dimensions, Phys. Rev. Lett. **98**, 106803 (2007).

[8] C. L. Kane and E. J. Mele, Z_2 Topological Order and the Quantum Spin Hall Effect, Phys. Rev. Lett. **95**, 146802 (2005).

[9] L. Fu, Topological Crystalline Insulators, Phys. Rev. Lett. **106**, 106802 (2011).

[10] A. H. Castro Neto, F. Guinea, N. M. R. Peres, K. S. Novoselov, and A. K. Geim, The electronic properties of graphene, Rev. Mod. Phys. **81**, 109 (2009).

[11] N. P. Armitage, E. J. Mele, and A. Vishwanath, Weyl and Dirac semimetals in three-dimensional solids, Rev. Mod. Phys. **90**, 015001 (2018).

[12] A. A. Burkov, M. D. Hook, and L. Balents, Topological nodal semimetals, Phys. Rev. B **84**, 235126 (2011).

[13] R. Bianco and R. Resta, Mapping topological order in coordinate space, Phys. Rev. B **84**, 241106(R) (2011).

[14] T. A. Loring and M. B. Hastings, Disordered topological insulators via C^*-algebras, Europhys. Lett. **92**, 67004 (2010).

[15] A. Kitaev, Anyons in an exactly solved model and beyond, Ann. Phys. (Amsterdam) **321**, 2 (2006).

[16] A. Cerjan and T. A. Loring, An operator-based approach to topological photonics, Nanophotonics **11**, 4765 (2022).

[17] J. Fan and H. Huang, Topological states in quasicrystals, Front. Phys. **17**, 13203 (2022).

[18] A. Agarwala and V. B. Shenoy, Topological Insulators in Amorphous Systems, Phys. Rev. Lett. **118**, 236402 (2017).

[19] R. Chen, C.-Z. Chen, J.-H. Gao, B. Zhou, and D.-H. Xu, Higher-Order Topological Insulators in Quasicrystals, Phys. Rev. Lett. **124**, 036803 (2020).

[20] Y.-B. Yang, T. Qin, D.-L. Deng, L.-M. Duan, and Y. Xu, Topological Amorphous Metals, Phys. Rev. Lett. **123**, 076401 (2019).

[21] H. Weyl, Elektron und gravitation. I, Z. Phys. **56**, 330 (1929).

[22] S. Y. Xu, I. Belopolski, N. Alidoust, M. Neupane, G. Bian, C. Zhang, R. Sankar, G. Chang, Z. Yuan, C. C. Lee, S.-M. Huang, H. Zheng, J. Ma, D. S. Sanchez, B. Wang, A. Bansil, F. Chou, P. P. Shibayev, H. Lin, S. Jia *et al.*, Discovery of a Weyl fermion semimetal and topological Fermi arcs, Science **349**, 613 (2015).

[23] B. Q. Lv, H. M. Weng, B. B. Fu, X. P. Wang, H. Miao, J. Ma, P. Richard, X. C. Huang, L. X. Zhao, G. F. Chen, Z. Fang, X. Dai, T. Qian, and H. Ding, Experimental Discovery of Weyl Semimetal TaAs, Phys. Rev. X **5**, 031013 (2015).

[24] L. Lu, Z. Wang, D. Ye, L. Ran, L. Fu, J. D. Joannopoulos, and M. Soljačić, Experimental observation of Weyl points, Science **349**, 622 (2015).

[25] X. Wan, A. M. Turner, A. Vishwanath, and S. Y. Savrasov, Topological semimetal and Fermi-arc surface states in the electronic structure of pyrochlore iridates, Phys. Rev. B **83**, 205101 (2011).

[26] G. E. Volovik, *The Universe in a Helium Droplet* (Clarendon Press, Oxford, 2003).

[27] M. Zhou, L. Ying, L. Lu, L. Shi, J. Zi, and Z. Yu, Electromagnetic scattering laws in Weyl systems, Nat. Commun. **8**, 1388 (2017).

[28] C. Guo, V. S. Asadchy, B. Zhao, and S. Fan, Light control with Weyl semimetals, eLight **3**, 2 (2023).

[29] D. Vanderbilt, *Berry Phases in Electronic Structure Theory* (Cambridge University Press, Cambridge, 2018).

[30] J. H. Pixley, J. H. Wilson, D. A. Huse, and S. Gopalakrishnan, Weyl Semimetal to Metal Phase Transitions Driven by Quasiperiodic Potentials, Phys. Rev. Lett. **120**, 207604 (2018).

[31] V. Mastropietro, Stability of Weyl semimetals with quasiperiodic disorder, Phys. Rev. B **102**, 045101 (2020).

[32] Y. Wang and S. Chen, Fate of Weyl semimetals in the presence of incommensurate potentials, Phys. Rev. A **95**, 053634 (2017).

[33] R. Penrose, The role of aesthetics in pure and applied mathematical research, Bull. Inst. Math. Appl. **10**, 266 (1974).

[34] We employ the word "dense" in the mathematical sense, i.e., a set is dense if in between any two elements one can always find at least one other element.

[35] N. G. de Bruijn, Algebraic theory of Penrose's non-periodic tilings of the plane. I, Indagationes Math. (Proc.) **84**, 39 (1981).

[36] O. Entin-Wohlman, M. Kléman, and A. Pavlovitch, Penrose tiling approximants, J. Phys. France **49**, 587 (1988).

[37] H. Tsunetsugu, T. Fujiwara, K. Ueda, and T. Tokihiro, Electronic properties of the Penrose lattice. I. Energy spectrum and wave functions, Phys. Rev. B **43**, 8879 (1991).

[38] See Supplemental Material at http://link.aps.org/supplemental/10.1103/PhysRevB.108.L121109 for more details.

[39] F. V. Babalievski, Percolation conductivity of Penrose lattices by the transfer-matrix Monte Carlo method, J. Non-Cryst. Solids **153-154**, 370 (1993).

[40] R. Ghadimi, T. Sugimoto, and T. Tohyama, Mean-field study of the Bose–Hubbard model in the Penrose lattice, Phys. Rev. B **102**, 224201 (2020).

[41] B. A. Bernevig and T. L. Hughes, *Topological Insulators and Topological Superconductors* (Princeton University Press, Princeton, NJ, 2013).

[42] C. Wang, F. Liu, and H. Huang, Effective Model for Fractional Topological Corner Modes in Quasicrystals, Phys. Rev. Lett. **129**, 056403 (2022).

[43] A. C. Potter, I. Kimchi, and A. Vishwanath, Quantum oscillations from surface Fermi arcs in Weyl and Dirac semimetals, Nat. Commun. **5**, 5161 (2014).

[44] P. J. W. Moll, N. L. Nair, T. Helm, A. C. Potter, I. Kimchi, A. Vishwanath, and J. G. Analytis, Transport evidence for Fermi-arc-mediated chirality transfer in the Dirac semimetal Cd₃As₂, Nature (London) **535**, 266 (2016).

[45] X.-L. Qi, Y.-S. Wu, and S.-C. Zhang, Topological quantization of the spin Hall effect in two-dimensional paramagnetic semiconductors, Phys. Rev. B **74**, 085308 (2006).

[46] Z.-R. Liu, C.-B. Hua, T. Peng, and B. Zhou, Chern insulator in a hyperbolic lattice, Phys. Rev. B **105**, 245301 (2022).

[47] X.-L. Qi and S.-C. Zhang, Topological insulators and superconductors, Rev. Mod. Phys. **83**, 1057 (2011).

[48] D.-T. Tran, A. Dauphin, N. Goldman, and P. Gaspard, Topological Hofstadter insulators in a two-dimensional quasicrystal, Phys. Rev. B **91**, 085125 (2015).

[49] D. Levine and P. J. Steinhardt, Quasicrystals. I. Definition and structure, Phys. Rev. B **34**, 596 (1986).

[50] Y. Yokoyama, Y. Yamada, K. Fukaura, H. Sunada, A. Inoue, and R. Note, Stable decagonal quasicrystal in an Al–Mn–Fe–Ge system, Jpn. J. Appl. Phys. **36**, 6470 (1997).

[51] T. T. Dorini, F. Brix, A. Chatelier, C. Kokalj, and E. Gaudry, Two-dimensional oxide quasicrystal approximants with tunable electronic and magnetic properties, Nanoscale **13**, 10771 (2021).

[52] C.-Z. Chang, J. Zhang, X. Feng, J. Shen, Z. Zhang, M. Guo, K. Li, Y. Ou, P. Wei, L.-L. Wang, Z.-Q. Ji, Y. Feng, S. Ji, X. Chen, J. Jia, X. Dai, Z. Fang, S.-C. Zhang, K. He, Y. Wang *et al.*, Experimental observation of the quantum anomalous Hall effect in a magnetic topological insulator, Science **340**, 167 (2013).

[53] Z. Wang, Y. Chong, J. D. Joannopoulos, and M. Soljačić, Observation of unidirectional backscattering-immune topological electromagnetic states, Nature (London) **461**, 772 (2009).

[54] Y. Zhang, Z. Lan, L. Hu, Y. Shu, X. Yuan, P. Guo, X. Peng, W. Chen, and J. Li, Chiral photonic topological states in Penrose quasicrystals, Opt. Lett. **48**, 2229 (2023).

[55] C. Qian, Y. Jiang, J. Jin, T. Christensen, M. Soljačić, A. V. Kildishev, and B. Zhen, Topological electromagnetic waves in dispersive and lossy plasma crystals, arXiv:2303.04903.

[56] L. M. Nash, D. Kleckner, A. Read, V. Vitelli, A. M. Turner, and W. T. M. Irvine, Topological mechanics of gyroscopic metamaterials, Proc. Natl. Acad. Sci. USA **112**, 14495 (2015).

[57] Y. Ding, Y. Peng, Y. Zhu, X. Fan, J. Yang, B. Liang, X. Zhu, X. Wan, and J. Cheng, Experimental Demonstration of Acoustic Chern Insulators, Phys. Rev. Lett. **122**, 014302 (2019).

[58] J. D. Cain, A. Azizi, M. A. Conrad, S. M. Griffin, and A. Zettl, Layer-dependent topological phase in a two-dimensional quasicrystal and approximant, Proc. Natl. Acad. Sci. USA **117**, 26135 (2020).

[59] T. Timusk, J. P. Carbotte, C. C. Homes, D. N. Basov, and S. G. Sharapov, Three-dimensional Dirac fermions in quasicrystals as seen via optical conductivity, Phys. Rev. B **87**, 235121 (2013).

[60] L. Bendersky, Quasicrystal with One-Dimensional Translational Symmetry and a Tenfold Rotation Axis, Phys. Rev. Lett. **55**, 1461 (1985).

[61] S. Aubry and G. André, Analyticity breaking and Anderson localization in incommensurate lattices, Ann. Isr. Phys. Soc. **3**, 18 (1980).

[62] R. Nandkishore, D. A. Huse, and S. L. Sondhi, Rare region effects dominate weakly disordered three-dimensional Dirac points, Phys. Rev. B **89**, 245110 (2014).

[63] J. H. Pixley, D. A. Huse, and S. Das Sarma, Rare-Region-Induced Avoided Quantum Criticality in Disordered Three-Dimensional Dirac and Weyl Semimetals, Phys. Rev. X **6**, 021042 (2016).

[64] T. A. Loring and H. Schulz-Baldes, Finite volume calculation of K-theory invariants, New York J. Math. **23**, 1111 (2017).

[65] H. Schulz-Baldes and T. Stoiber, Invariants of disordered semimetals via the spectral localizer, Europhys. Lett. **136**, 27001 (2021).

[66] H. B. Nielsen and M. Ninomiya, Absence of neutrinos on a lattice: (I). Proof by homotopy theory, Nucl. Phys. B **185**, 20 (1981).

[67] H. B. Nielsen and M. Ninomiya, Absence of neutrinos on a lattice: (II). Intuitive topological proof, Nucl. Phys. B **193**, 173 (1981).

[68] B. Bradlyn, J. Cano, Z. Wang, M. Vergniory, C. Felser, R. J. Cava, and B. A. Bernevig, Beyond Dirac and Weyl fermions: Unconventional quasiparticles in conventional crystals, Science **353**, aaf5037 (2016).

[69] F. Tang and X. Wan, Exhaustive construction of effective models in 1651 magnetic space groups, Phys. Rev. B **104**, 085137 (2021).

[70] Z.-M. Yu, Z. Zhang, G.-B. Liu, W. Wu, X.-P. Li, R.-W. Zhang, S. A. Yang, and Y. Yao, Encyclopedia of emergent particles in three-dimensional crystals, Sci. Bull. **67**, 375 (2022).